Emergence of Active Nematic Behavior in Monolayers of Isotropic Cells

Romain Mueller, Julia M. Yeomans, and Amin Doostmohammadi*
The Rudolf Peierls Centre for Theoretical Physics, Clarendon Laboratory, Parks Road, University of Oxford, Oxford OX1 3PU, United Kingdom

(Received 30 October 2018; published 1 February 2019)

There is now growing evidence of the emergence and biological functionality of liquid crystal features, including nematic order and topological defects, in cellular tissues. However, how such features that intrinsically rely on particle elongation emerge in monolayers of cells with isotropic shapes is an outstanding question. In this Letter, we present a minimal model of cellular monolayers based on cell deformation and force transmission at the cell-cell interface that explains the formation of topological defects and captures the flow-field and stress patterns around them. By including mechanical properties at the individual cell level, we further show that the instability that drives the formation of topological defects, and leads to active turbulence, emerges from a feedback between shape deformation and active driving. The model allows us to suggest new explanations for experimental observations in tissue mechanics, and to propose designs for future experiments.

DOI: 10.1103/PhysRevLett.122.048004

The collective migration of cells plays a crucial role in vital physiological processes, and there is rapidly growing interest in studying the interplay between mechanics and the collective behavior of cells at the tissue level [1]. Experimental studies have uncovered the important role of mechanical forces in wound healing [2], morphogenesis [3], and cancer invasion [4]. Interestingly, many cellular systems display properties of liquid crystals such as local nematic alignment and the appearance of topological defects—singular points in the cellular alignment where the orientational order vanishes. Important examples are elongated fibroblasts at high densities [5], monolayers of epithelial cells such as Madin-Darby Canine Kidney (MDCK), human breast cancer cells (MCF-7) [6], and Human Bronchial Cells (HBC) [7], dense cultures of amoeboid cells [8], and neural progenitor stem cells [9]. However, unlike classic liquid crystals, these systems are "active," constantly being driven out of equilibrium by the motion of individual cells within the tissue.

There is emerging evidence that the collective dynamics of epithelial cells can be captured by theories of active liquid crystals [5–7,9,10]. For example, flows around cellular division events in epithelial cells and the transition to shear flows in confined fibroblast cells have been reproduced by such a theory [5,11], and large-scale velocity fields measured in monolayers of epithelial and endothelial cells show long-range flows and patterns of localized vorticity reminiscent of the turbulent state observed in active nematic liquid crystals at high activity [7,12–14]. More recently, the properties of nematic topological defects, which can control death and extrusion in monolayers of MDCK cells [6], were shown to be consistent with an active nematic description. Such a connection is highly surprising because individual epithelial cells on a substrate have a well-defined direction of movement (polarity), and cells in a monolayer are on average isotropic in shape. Therefore, it is far from obvious how the observed nematic features of the tissue can emerge from the collective dynamics. Because most theoretical studies of epithelial cells have concentrated on polar driving [15,16] or have neglected shape deformations altogether [17–19], much remains to be explored in order to understand how such macroscopic nematic features relate to the microscopic dynamics in cellular monolayers.

In this Letter, we show that the local deformation of cells provides a suitable nematic order parameter even in systems where cells are not naturally elongated. Using a simple microscopic model of dense two-dimensional cellular layers that captures single-cell deformations, we find that a minimal form of microscopic dipolar interaction between cells based on their deformations leads to spontaneous symmetry breaking and drives the system out of equilibrium. At high activities, we also observe the proliferation of topological defects in the orientation field and the emergence of active turbulent flows as observed in monolayers of epithelial cells [6,7]. We further show that the experimentally observed patterns of flows and mechanical stresses around topological defects are accurately captured by our modeling framework.

The main goal of our study is to consider the impact of intercellular stresses that are generated due to cell-cell interactions in regulating the collective behavior in cellular tissues, as highlighted by recent experiments on epithelial cells [20]. We model cells as active deformable droplets in two dimensions using a phase-field model. The phase-field approach has been widely applied to problems involving

single cells (see Ref. [21] for a review) and more recently to the description of a few migrating cells [22] and the study of confluent epithelia [23–26]. We start by describing an epithelium consisting of N cells using a different phase field ϕ_i for each individual cell. Values of $\phi_i = 1$ and $\phi_i = 0$ denote the interior and the exterior of a cell, respectively, and the cell boundary is defined to lie at the midpoint $\phi_i = 1/2$. We define the dynamics of the fields ϕ_i as

$$\partial_t \phi_i + \mathbf{v}_i \nabla \phi_i = -\frac{\delta \mathcal{F}}{\delta \phi_i}, \qquad i = 1, \ldots, N, \tag{1}$$

where $\mathcal{F}$ is a free energy and $\mathbf{v}_i$ is the total velocity of cell i. This velocity enters Eq. (1) only through the advection term, effectively pushing each cell uniformly as a whole without inducing any deformation of its interface.

The free energy $\mathcal{F}$ defines the dynamics of the individual interfaces and is written as $\mathcal{F} = \mathcal{F}_{\mathrm{CH}} + \mathcal{F}_{\mathrm{area}} + \mathcal{F}_{\mathrm{rep}}$, where

$$\begin{aligned}
\mathcal{F}_{\mathrm{CH}} &= \sum_i \frac{\gamma}{\lambda} \int d\mathbf{x}\, \{4\phi_i^2(1-\phi_i)^2 + \lambda^2 (\nabla \phi_i)^2\}, \\
\mathcal{F}_{\mathrm{area}} &= \sum_i \mu \left(1 - \frac{1}{\pi R^2} \int d\mathbf{x}\ \phi_i^2\right)^2, \\
\mathcal{F}_{\mathrm{rep}} &= \sum_i \sum_{j \neq i} \frac{\kappa}{\lambda} \int d\mathbf{x}\, \phi_i^2 \phi_j^2.
\end{aligned} \tag{2}$$

The Cahn-Hilliard free energy $\mathcal{F}_{\mathrm{CH}}$ stabilizes the cell interface. Our formulation is guided by simplicity but could be replaced by more realistic models of the cellular boundary [27–29]. The contribution $\mathcal{F}_{\mathrm{area}}$ provides a soft constraint for the area of the individual cells around the value πR^2, where R is the cell radius, such that the cells are compressible [30]. Finally, the repulsion term $\mathcal{F}_{\mathrm{rep}}$ penalizes regions where two cells overlap. Normalization has been chosen such that the width of the interfaces at equilibrium is λ and such that the properties of the cells are roughly preserved when λ is rescaled (see Supplemental Material [31]). The parameters γ, μ, and κ set the relaxation timescale of shape deformations, area changes, and repulsive forces, respectively (see Supplemental Material [31] for the parameter values).

This formulation allows the cellular interfaces to be resolved, and intracellular forces to be defined at the microscopic level [Fig. 1(b)]. There are many physical forces of importance at the cellular level [32,33], and force transmission between cells has been shown to contribute to collective phenomena such as collective durotaxis [34] or coordination during morphogenesis [35,36] and wound healing [2,37]. We concentrate here on a simplified description and consider only substrate friction and forces generated at the cellular interfaces, leading to the force balance equation:

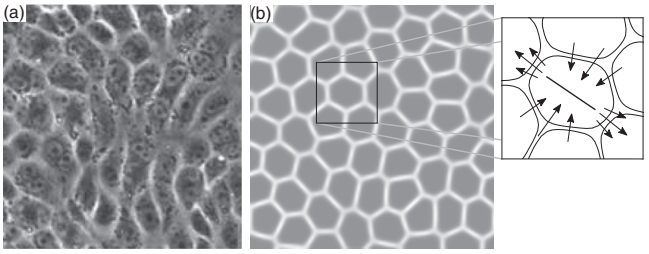

FIG. 1. (a) A microscope image of a MDCK monolayer (adapted from Ref. [11]) and (b) a simulation snapshot. Interfaces between cells are defined as the overlap of the phase fields $\sum_{i \neq j} \phi_i \phi_j$ (left). Contours $\phi_i = 1/2$ with an illustration of the principal axis of the deformation tensor together with the resulting dipolar force density (right). The director of the dipolar force is parallel to the main deformation axis.

$$\xi \mathbf{v}_i = \mathbf{F}_i^{\mathrm{int}}, \tag{3}$$

where ξ is a substrate friction coefficient and $\mathbf{F}_i^{\mathrm{int}}$ is the total force acting on the interface of cell i. By analogy with continuum theories, we define these microscopic interface forces in terms of a macroscopic tissue stress tensor σ_{tissue} as

$$\mathbf{F}_i^{\mathrm{int}} = \int d\mathbf{x}\, \phi_i \boldsymbol{\nabla} \cdot \boldsymbol{\sigma}_{\mathrm{tissue}} = -\int d\mathbf{x}\, \boldsymbol{\sigma}_{\mathrm{tissue}} \cdot \boldsymbol{\nabla} \phi_i. \tag{4}$$

The first expression is the integral of the local force $\boldsymbol{\nabla} \cdot \boldsymbol{\sigma}_{\mathrm{tissue}}$ weighted by the phase field ϕ_i, while the second is the integral of the force exerted by the stress tensor on the vector $-\nabla \phi_i$ normal to the interface and pointing outwards. Equation (4) effectively bridges scales between local forces at the level of the individual cells and properties of the whole tissue.

Equations (1)–(4) define a generic model of two-dimensional epithelial monolayers that only requires an appropriate definition of the stress tensor as input. Following our analogy with continuum theories, we introduce the usual separation into passive and active stresses

$$\sigma_{\mathrm{tissue}} = -P\mathbb{I} - \zeta \mathbf{Q}, \tag{5}$$

where the fields P and $\mathbf{Q}$ are the tissue pressure and tissue nematic tensor to be defined below. As pointed out in Ref. [25], there is in fact much freedom in defining P from the total free energy $\mathcal{F}$. Here we use the thermodynamically consistent definition

$$P = \sum_i \left(\frac{\delta \mathcal{F}_{\mathrm{rep}}}{\delta \phi_i} - \frac{\delta \mathcal{F}_{\mathrm{CH}}}{\delta \phi_i} - \frac{\delta \mathcal{F}_{\mathrm{area}}}{\delta \phi_i} \right), \tag{6}$$

which includes contributions from compression and surface tension terms (see Supplemental Material [31] for details). Key to our results is the definition of the tissue nematic tensor in Eq. (5), which is based on the following cell deformation:

$$\mathbf{Q} = \sum_i \phi_i \mathbf{S}_i, \tag{7}$$

where $\mathbf{S}_i$ is the deformation tensor of cell i [38] defined as the traceless part of $-\int d\mathbf{x}\,(\nabla\phi_i)^{\mathsf{T}}\nabla\phi_i$. Its eigenvalues and eigenvectors measure the strength and orientation of the main deformation axes of cell i (see Supplemental Material [31] for details). Multiplying each deformation tensor by the corresponding phase field ensures that $\mathbf{Q}$ is a field defined at each point in space (see Supplemental Material, Fig. 9.).

We now turn to the main focus of this Letter and show that introducing a local active term proportional to the deformation of single cells is able to drive the system out of equilibrium and to capture the active nematic phenomenology of dense cellular monolayers. From Eqs. (4), (5), one can see that the active term, $\zeta\mathbf{Q}$, for a given nematic tensor $\mathbf{Q}$ can be interpreted as a dipolar force density distributed along the cells' interfaces while P is a simple elastic repulsion force. As a result, each cell pushes or pulls its neighbors depending on the direction of their contact area with respect to the stress tensor (see Fig. 1 for an illustration). Note however that this is an effect of the cellular interactions alone: single, isolated, cells do not deform at nonvanishing activity.

This simple definition of the tissue nematic tensor in terms of the local deformation is able to create large-scale flows for high enough activity strengths and leads to the spontaneous creation of defects in the nematic field (see Supplemental Material [31], Movie 1). Defining the tissue velocity as $\mathbf{v} = \sum_i \phi_i \mathbf{v}_i$, we see that the root-mean-square velocity $v_{\mathrm{rms}}^2 = \langle \mathbf{v}^2 \rangle$ and nematic order $S_{\mathrm{rms}}^2 = \langle \det \mathbf{S}^2 \rangle = \langle S_{11}^2 + S_{12}^2 \rangle$ develop nonzero values as ζ is increased [Fig. 2(a) and Supplemental Material, Fig. 6], indicating that our model shows an activity-driven transition to nonzero nematic order and flows. Because of the nematic nature of the interactions, the total force is approximately zero at the tissue level and the system does not develop any system-wide net velocity under periodic boundary conditions. In particular this means the transition to collective movement here is different from the flocking phase transitions observed in Vicsek-type active systems with polar driving.

The transition to flow shows a clear activity threshold which depends in a well-defined manner on the elasticity γ [Fig. 2(b)], but is independent of the domain size L [Fig. 2(c)]. This is in contrast to continuum models of active nematics, which explicitly include the velocity as a hydrodynamic variable and where a hydrodynamic instability initiates flows at an activity threshold that tends to zero as $L \to \infty$ [39]. This suggests a different origin for the transition and we conjecture that it is driven by the interaction forces at the cell-cell interfaces that amplify the deformation for extensile activity ($\zeta > 0$) in our model. This hypothesis is strengthened by the fact that the system is stable for contractile activity ($\zeta < 0$) for which the interactions at the interfaces tend to restore the equilibrium shape (Supplemental Material Fig. 7). A finite value of the threshold then appears because cells need to push (pull) strongly enough to cause sufficient deformation of their neighbors. Using the balance of active stresses with the pressure contribution due to the elastic energetic cost of cell deformation, the activity threshold is found to depend linearly on the elasticity, $\zeta_{\mathrm{cr}} \sim \gamma$, consistent with the simulation results [Fig. 2(b)], see Supplemental Material [31] for more details.

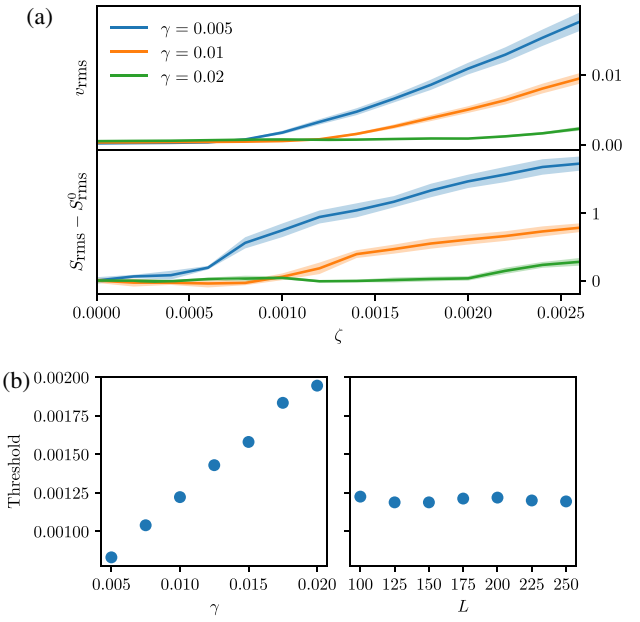

FIG. 2. Transition to flows in an extensile system of 240 cells. (a) The root-mean-square velocity v_{rms} and nematic order S_{rms} develop nonzero values with increasing activity ζ, where the mean value is taken over each individual cell. Note that we subtracted the zero-activity rms order $S^0_{\mathrm{rms}} = S_{\mathrm{rms}}|_{\zeta=0}$. Mean $\pm$ std from five simulations. (b) Dependence of the location of the activity threshold on the elasticity γ and domain size L. The threshold is defined as the first value of activity ζ for which the $v_{\mathrm{rms}} > 10^{-7}$ after 3000 simulation steps, after v_{rms} has been averaged over four simulations.

These differences in the origin of the spontaneous flow generation have clear observable consequences for the dynamics of the system. In particular, we do not observe the formation of highly distorted lines in the nematic field —"walls"—that are a typical consequence of the hydrodynamic instability [40,41]. This in turn affects the mechanism by which nematic defects are spontaneously created. While in continuum active nematics defect proliferation is predominantly mediated by the unzipping of walls by pairs of oppositely charged defects [40], the emergence of defect pairs occurs spontaneously at random positions in our cell-based model. Interestingly this resembles much more closely the experimental observations of the defect proliferation in MDCK cells where it has been puzzling that no walls are apparent [6].

Spontaneous defect pair creation leads to the emergence of a state resembling the active turbulence observed in continuum theories of active nematics [40] (see Supplmental Material [31], Movie 2). The vorticity autocorrelation function $C_\omega(r) = \langle \omega(r)\omega(0)\rangle / \langle \omega(0)^2 \rangle$ for different values of the activity shows a well-defined length scale determined by the minimum of $C_\omega(r)$ [Fig. 3(a)]. Autocorrelation functions for the velocity and the nematic field show similar behavior (see Supplemental Material, Figs. 4 and 5). This indicates that force transmission mediated by cell-cell contacts leads to long-range flows at macroscopic scales. Increasing activity ζ leads to smaller vortices, while increasing elasticity γ results in larger vortices [Figs. 3(b) and 3(c)]. In addition, consistent with continuum hydrodynamic models [42,43], defects are always created and annihilated in pairs and defect density and defect creation rate both increase with increasing activity ζ (Supplemental Material, Fig. 8).

Finally, we analyzed the properties of flows and stresses around defects, which are crucial in determining the dynamics of active turbulence [40]. In particular, the isotropic stress patterns around $+1/2$ defects were found to work as a mechanotransduction pathway to control cell death and its subsequent expulsion from an epithelial monolayer [6]. Figure 4 shows the isotropic stress patterns and flow fields around $\pm 1/2$ defects obtained from the cell-based model. These agree very well with the analytical prediction of flow fields around isolated defects [44,45], as well as with recent experimental measurements of defects flow fields and isotropic stresses in epithelial monolayers [6].

Together, our results demonstrate that a cell-based model which accounts for cell deformability and force transmission at cell-cell contacts can serve as a minimal and generic model to explain the active liquid crystal properties found recently in epithelial monolayers. The model reproduces the phenomenology of active liquid crystals, together with mechanical stress and flow patterns consistent with experimental measurements. It explains that a bootstrap feedback between shape deformations and intercellular driving allows cells of isotropic shape, such as MDCK cells or nonaggressive human breast cancer cells (MCF-7), to drive an instability to spontaneous flow and to create topological defects. Even though our model is based on a force-balance formulation, in the macroscopic limit, it shows clear hydrodynamic behavior due to the long-range interactions mediated by cell-cell contacts.

Our minimal model leads to a number of testable predictions that could challenge current understanding in tissue mechanics. Even though individual cells are internally made of contractile material [46], there is now clear evidence that their macroscopic collective behavior can show properties of extensile nematic theories [6,7], but the underlying mechanism remains controversial. Here, we predict that such a coarse-grained extensility can arise from interactions between the cells. High resolution measurements of the

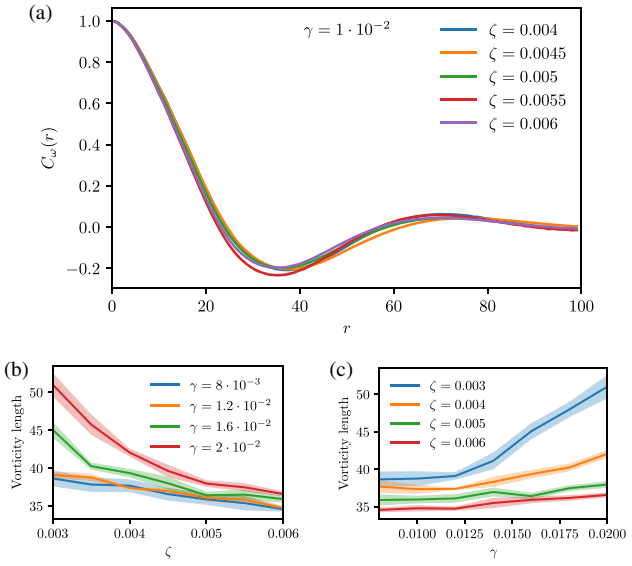

FIG. 3. Properties of flows during active turbulence for an extensile system. (a) Spatial autocorrelation function $C_\omega(r) = \langle \omega(r)\omega(0)\rangle / \langle \omega(0)^2 \rangle$ of the vorticity for different values of ζ. (b)–(c) Dependence of the vorticity length, defined as the location of the minimum of the vorticity autocorrelation function, as a function of activity ζ and elasticity γ. Mean $\pm$ std from five simulations.

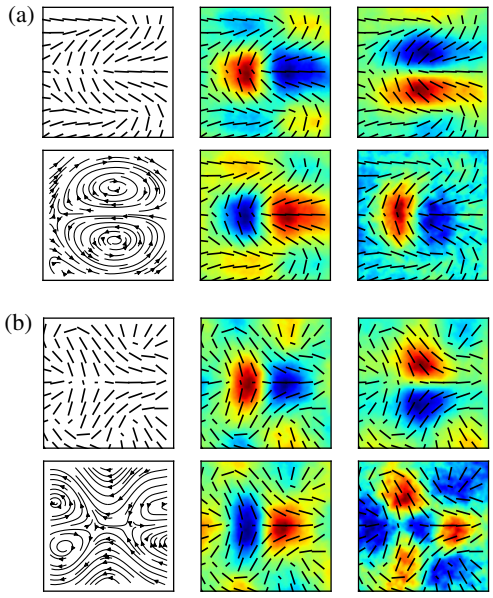

FIG. 4. Average properties of $+1/2$ (a) and $-1/2$ (b) defects in an extensile system with $\zeta = 5 \times 10^{-3}$ and $\gamma = 1.4 \times 10^{-2}$: nematic field (top left), flow field (bottom left), σ_{xx} (top center), σ_{yy} (bottom center), σ_{xy} (top right), pressure (bottom right). Colors are normalized such that the maximum value is red and the minimum value is blue. Averaging was performed over five simulations. Each box shows a domain of size 100×100 and corresponds to approximately 60 cells.

forces acting on individual cells within a confluent monolayer can test this theory and further shed light on the force transmission mechanism. Furthermore, the existence of an activity threshold can be examined in experiments by introducing incremental dosages of drugs that impair the cell motility and molecular perturbations that affect cell deformability.

R. M. was supported by Grant No. P2EZP2_165261 of the Swiss National Science Foundation. A. D. was supported by a Royal Commission for the Exhibition of 1851 Research Fellowship.

*amin.doostmohammadi@physics.ox.ac.uk

[1] B. Ladoux and R.-M. Mège, Nat. Rev. Mol. Cell Biol. **18**, 743 (2017).
[2] A. Brugués, E. Anon, V. Conte, J. H. Veldhuis, M. Gupta, J. Colombelli, J. J. Muñoz, G. W. Brodland, B. Ladoux, and X. Trepat, Nat. Phys. **10**, 683 (2014).
[3] K. Chiou and E. S. Collins, Dev. Biol. **433**, 155 (2018).
[4] P. Friedl, J. Locker, E. Sahai, and J. E. Segall, Nat. Cell Biol. **14**, 777 (2012).
[5] G. Duclos, C. Blanch-Mercader, V. Yashunsky, G. Salbreux, J.-F. Joanny, J. Prost, and P. Silberzan, Nat. Phys. **14**, 728 (2018).
[6] T. B. Saw, A. Doostmohammadi, V. Nier, L. Kocgozlu, S. Thampi, Y. Toyama, P. Marcq, C. T. Lim, J. M. Yeomans, and B. Ladoux, Nature (London) **544**, 212 (2017).
[7] C. Blanch-Mercader, V. Yashunsky, S. Garcia, G. Duclos, L. Giomi, and P. Silberzan, Phys. Rev. Lett. **120**, 208101 (2018).
[8] H. Gruler, U. Dewald, and M. Eberhardt, Eur. Phys. J. B **11**, 187 (1999).
[9] K. Kawaguchi, R. Kageyama, and M. Sano, Nature (London) **545**, 327 (2017).
[10] J. Prost, F. Jülicher, and J.-F. Joanny, Nat. Phys. **11**, 111 (2015).
[11] A. Doostmohammadi, S. P. Thampi, T. B. Saw, C. T. Lim, B. Ladoux, and J. M. Yeomans, Soft Matter **11**, 7328 (2015).
[12] M. Poujade, E. Grasland-Mongrain, A. Hertzog, J. Jouanneau, P. Chavrier, B. Ladoux, A. Buguin, and P. Silberzan, Proc. Natl. Acad. Sci. U. S. A. **104**, 15988 (2007).
[13] L. Petitjean, M. Reffay, E. Grasland-Mongrain, M. Poujade, B. Ladoux, A. Buguin, and P. Silberzan, Biophys. J. **98**, 1790 (2010).
[14] N. S. Rossen, J. M. Tarp, J. Mathiesen, M. H. Jensen, and L. B. Oddershede, Nat. Commun. **5**, 5720 (2014).
[15] D. Bi, X. Yang, M. C. Marchetti, and M. L. Manning, Phys. Rev. X **6**, 021011 (2016).
[16] D. L. Barton, S. Henkes, C. J. Weijer, and R. Sknepnek, PLoS Comput. Biol. **13**, e1005569 (2017).
[17] N. S. Gov, HFSP J. **3**, 223 (2009).
[18] P. Lee and C. Wolgemuth, PLoS Comput. Biol. **7**, e1002007 (2011).
[19] P. Lee and C. Wolgemuth, Phys. Rev. E **83**, 061920 (2011).
[20] E. Sadeghipour, M. A. Garcia, W. J. Nelson, and B. L. Pruitt, eLife **7**, e39640 (2018).
[21] In *Physical Models of Cell Motility*, edited by I. S. Aranson (Springer International Publishing, Switzerland, 2016).
[22] S. Najem and M. Grant, Phys. Rev. E **93**, 052405 (2016).
[23] M. Basan, J. Elgeti, E. Hannezo, W.-J. Rappel, and H. Levine, Proc. Natl. Acad. Sci. U.S.A. **110**, 2452 (2013).
[24] N. Sepúlveda, L. Petitjean, O. Cochet, E. Grasland-Mongrain, P. Silberzan, and V. Hakim, PLoS Comput. Biol. **9**, e1002944 (2013).
[25] B. Palmieri, Y. Bresler, D. Wirtz, and M. Grant, Sci. Rep. **5**, 11745 (2015).
[26] Y. Bresler, B. Palmieri, and M. Grant, arXiv:1807.07836v1.
[27] W. Helfrich, Z. Naturforsch. C **28**, 693 (1973).
[28] D. Shao, W.-J. Rappel, and H. Levine, Phys. Rev. Lett. **105**, 108104 (2010).
[29] T. Biben and C. Misbah, Phys. Rev. E **67**, 031908 (2003).
[30] Even though epithelial cells are rather incompressible in 3D, they are effectively compressible in 2D because they can stretch in the direction normal to the substrate plane.
[31] See Supplemental Material at http://link.aps.org/supplemental/10.1103/PhysRevLett.122.048004 more details on the model and its implementation.
[32] E. K. Paluch, C. M. Nelson, N. Biais, B. Fabry, J. Moeller, B. L. Pruitt, C. Wollnik, G. Kudryasheva, F. Rehfeldt, and W. Federle, BMC Biol. **13**, 47 (2015).
[33] P. Roca-Cusachs, V. Conte, and X. Trepat, Nat. Cell Biol. **19**, 742 (2017).
[34] R. Sunyer, V. Conte, J. Escribano, A. Elosegui-Artola, A. Labernadie, L. Valon, D. Navajas, J. M. Garcia-Aznar, J. J. Munoz, P. Roca-Cusachs, and X. Trepat, Science **353**, 1157 (2016).
[35] C. Guillot and T. Lecuit, Science **340**, 1185 (2013).
[36] R. Etournay, M. Popović, M. Merkel, A. Nandi, C. Blasse, B. Aigouy, H. Brandl, G. Myers, G. Salbreux, F. Jülicher, and S. Eaton, eLife **4**, e07090 (2015).
[37] F. Bosveld, I. Bonnet, B. Guirao, S. Tlili, Z. Wang, A. Petitalot, R. Marchand, P.-L. Bardet, P. Marcq, F. Graner, and Y. Bellaiche, Science **336**, 724 (2012).
[38] M. Asipauskas, M. Aubouy, J. A. Glazier, F. Graner, and Y. Jiang, Granular Matter **5**, 71 (2003).
[39] R. Aditi Simha and S. Ramaswamy, Phys. Rev. Lett. **89**, 058101 (2002).
[40] L. Giomi, M. J. Bowick, X. Ma, and M. C. Marchetti, Phys. Rev. Lett. **110**, 228101 (2013).
[41] S. P. Thampi, R. Golestanian, and J. M. Yeomans, Europhys. Lett. **105**, 18001 (2014).
[42] L. Giomi, Phys. Rev. X **5**, 031003 (2015).
[43] A. J. Vromans and L. Giomi, Soft Matter **12**, 6490 (2016).
[44] L. Giomi, L. Mahadevan, B. Chakraborty, and M. Hagan, Nonlinearity **25**, 2245 (2012).
[45] L. Giomi, M. J. Bowick, P. Mishra, R. Sknepnek, and M. C. Marchetti, Phil. Trans. R. Soc. A **372**, 20130365 (2014).
[46] W. Pomp, K. Schakenraad, H. E. Balcıoğlu, H. van Hoorn, E. H. J. Danen, R. M. H. Merks, T. Schmidt, and L. Giomi, Phys. Rev. Lett. **121**, 178101 (2018).